

Article

Phytoremediation of Soil Contaminated with Lithium Ion Battery Active Materials—A Proof-of-Concept Study

Jonas Henschel ¹, Maximilian Mense ¹, Patrick Harte ¹, Marcel Diehl ¹, Julius Buchmann ¹, Fabian Kux ¹, Lukas Schlatt ², Uwe Karst ², Andreas Hensel ³, Martin Winter ^{1,4} and Sascha Nowak ^{1,*}

¹ MEET Battery Research Center, University of Münster, Corrensstraße 46, 48149 Münster, Germany; jonas.henschel@uni-muenster.de (J.H.); maximilian.mense@uni-muenster.de (M.M.); patrick.harte@uni-muenster.de (P.H.); marcel.diehl@uni-muenster.de (M.D.); julius.buchmann@uni-muenster.de (J.B.); f_kux002@uni-muenster.de (F.K.); martin.winter@uni-muenster.de (M.W.)

² Institute of Inorganic and Analytical Chemistry, University of Münster, Corrensstraße 28/30, 48149 Münster, Germany; l_schl21@uni-muenster.de (L.S.); uk@uni-muenster.de (U.K.)

³ Institute for Pharmaceutical Biology and Phytochemistry, University of Münster, Corrensstraße 48, 48149 Münster, Germany; ahensel@uni-muenster.de

⁴ Helmholtz-Institute Münster, IEK-12, Forschungszentrum Jülich, Corrensstraße 46, 48149 Münster, Germany

* Correspondence: sascha.nowak@uni-muenster.de; Tel.: +49-251-83-36735

Received: 21 August 2020; Accepted: 29 September 2020; Published: 10 October 2020



Abstract: The lithium-ion battery is the most powerful energy storage technology for portable and mobile devices. The enormous demand for lithium-ion batteries is accompanied by an incomplete recycling loop for used lithium-ion batteries and excessive mining of Li and transition metals. The hyperaccumulation of plants represents a low-cost and green technology to reduce environmental pollution of landfills and disused mining regions with low environmental regulations. To examine the capabilities of these approaches, the hyperaccumulation selectivity of *Alyssum murale* for metals in electrode materials (Ni, Co, Mn, and Li) was evaluated. Plants were cultivated in a conservatory for 46 days whilst soils were contaminated stepwise with dissolved transition metal species via the irrigation water. Up to 3 wt% of the metals was quantified in the dry matter of different plant tissues (leaf, stem, root) by means of inductively coupled plasma-optical emission spectroscopy after 46 days of exposition time. The lateral distribution was monitored by means of micro X-ray fluorescence spectroscopy and laser ablation-inductively coupled plasma-mass spectrometry, revealing different storage behaviors for low and high metal contamination, as well as varying sequestration mechanisms for the four investigated metals. The proof-of-concept regarding the phytoextraction of metals from $\text{LiNi}_{0.33}\text{Co}_{0.33}\text{Mn}_{0.33}\text{O}_2$ cathode particles in the soil was demonstrated.

Keywords: hyperaccumulation; remediation; lithium-ion battery; lithium; transition metals; *Alyssum murale*; Laser ablation; μ -XRF

1. Introduction

Lithium-ion batteries (LIBs) represent the most promising electrical energy storage system for mobile applications due to their superior properties compared to other secondary batteries [1–3]. Consequently, sales figures of LIBs increased drastically in recent years whilst fields of application diverged [4,5]. Since then, and despite several recent innovative approaches, the recycling of used LIBs has fallen short of expectations, and a closed industrial recycling loop has not been established [6–9].

Furthermore, a recycling quota based on weight proportions primarily results in the recovery of cell housing materials. The recycling of Ni-, Co-, Mn-, and Cu-containing electrodes in hydro-metallurgical processes after the already established pyro-metallurgical fractionation is hardly economically feasible to the present state, and the lithium is lost in slag [10,11]. Consequently, the export of used batteries and the excessive mining of Co lead to environmental pollution of landfills, repositories, and disused mining regions due to low environmental regulations. In recent years, layered positive electrode materials based on Ni, Co, and Mn have been increasingly used in LIBs. It started with $\text{LiNi}_{0.33}\text{Co}_{0.33}\text{Mn}_{0.33}\text{O}_2$ (NCM111), whereas for present and future battery cell generations, trends show an increase in Ni contents and a decrease in Co contents [12,13]. As a consequence, the recycling of Co can contribute to the compensation of future Co demands [14].

The capability of the hyperaccumulation of metals in plants can be used for reverse environmental contamination and to contribute to an improved recycling loop. The accumulation and tolerance of high metal concentrations (by a factor of 50–100 higher than normal) of certain species represent a selection advantage in terms of (i) an elemental-defense strategy against herbivores and pathogens, (ii) drought stress protection, (iii) physiological benefits, and (iv) allelopathic effects in the habitat [15–17]. Many species of hyperaccumulators belong to the family of Brassicaceae, Euphorbiaceae, and Asteraceae. An increased metal transporter abundance and chelating agents (organic acids, peptides) facilitating transport and sequestration are fundamental principles for hyperaccumulation [18]. The hypertolerance toward toxic metals can be explained by (I) detoxification by complexation, (II) metal sequestration in cellular compartments, and (III) metal sequestration via exocellular deposition [19]. The capability of hyperaccumulation for Ni^{2+} , Co^{2+} , and Mn^{2+} ions was described for different species, and the application of plants for the detoxification of soils has been demonstrated (phytoremediation) [19–24]. This low-cost and green technology constitutes a valuable niche compared to expensive conventional soil remediation approaches. Furthermore, the utilization of the hyperaccumulation can be conveyed to economical phytomining concepts if plants are able to develop biomass quickly and can be cultivated and harvested easily [25–27]. The Ni hyperaccumulator *Alyssum murale* Waldst. & Kit. (engl. silver alyssum, yellow tuft) (Brassicaceae) has been investigated intensively regarding the accumulation capabilities of the species, as well as for the potential uptake mechanism for Ni and Co. From these investigations, *A. murale* has become a ‘model organism’ in this context [19,28–30]. Besides microscopy, laser ablation- and X-ray-based techniques are valuable tools for the visualization of the hyperaccumulation of metals by plants [31–34]. In particular, the simultaneous accumulation capabilities for Ni and Co were critical for the examination of *A. murale* in this work [19,35].

In this study, the hyperaccumulation of the transition metals present in LIB positive electrode materials (Ni, Co, and Mn) was investigated using *A. murale*. In the first step, (a) the selectivity, (b) uptake capabilities, (c) localization in plant tissues, and (d) reduction in transition metals in the soil after contamination in three different degrees were examined. In the second step, a proof-of-concept was conducted after pH-dependent dissolution experiments with LIB ash containing NCM111 to determine dissolved transition metal amounts. Subsequently, soils were contaminated with low concentrations of pristine NCM111 to simulate realistic conditions and a natural dissolution behavior of the electrode material, as well as short exposition times for *alyssum murale*. Additionally, the uptake of Li, as a crucial component of LIBs, was monitored within this study.

2. Results and Discussion

2.1. Hyperaccumulation of Ni, Co, and Mn in *Alyssum Murale*

A. murale is a model plant for the hyperaccumulation of metals, particularly of Ni [16]. For the implementation in phytoremediation approaches at LIB landfill sites or disused mines, the selectivity toward Mn and the economically more valuable and toxic transition metal Co need to be considered. Furthermore, (i) tolerable metal expositions, (ii) metal uptake capabilities, (iii) localization in different plant tissues, as well as (iv) reduction in the soil after an accumulation phase were examined for all

three metals. The advantage of the watering study was the controlled, stepwise addition of active, bioavailable metal cations. The respective contamination was increased continuously with every watering step (three contamination levels: 10, 50, and 250 mg metal with each step, Table 1). The first appearance of phenotypical intoxications (e.g., chlorosis, drying up of the leaves, and leaf loss) was observed after the exposure to a total of 1.75 g Ni and Co (level 3, day 14) for a single plant. For Mn, a dieback of *A. murale* occurred after the addition of 2.50 g Mn (level 3, day 20). Hence, the tolerable exposure for the respective metal was determined. In general, the plant growth was reduced for higher transition metal contaminations; watering at level 3 (5.0 g L⁻¹) resulted in crystallization effects on the soil surface (Figure S1). After a contamination phase of 20 days, ICP-OES was performed with leaves, stems, roots, and soils. The quantitative results are depicted in Table 1. After a contamination time of 20 days, all transition metals accumulated in high concentrations in the plant material (close to one-digit wt% and higher). The translocation process of the nickel from the root to leaf was highly effective and showed hyperaccumulation for levels 2 and 3 (Table 1, yellow).

Table 1. Concentrations of Ni, Co, and Mn (wt%) in different organs after 20 days of contamination with defined amounts of Ni, Co, and Mn of *A. murale* by means of ICP-OES regarding dry matter and dried soil. Highest concentrations in plants for the respective metals are indicated with different colors, and the natural occurrence of Mn in the control group is depicted in grey (n = 3).

Contamination Group	Sample	Ni/wt%	Co/wt%	Mn/wt%
Control	Leaf	<LOD	<LOD	0.02 (±0.00)
	Stem	<LOD	<LOD	<LOD
	Root	<LOD	<LOD	<LOD
	Soil	<LOD	<LOD	0.02 (±0.00)
Level 1	Leaf	0.04 (±0.00)	0.06 (±0.00)	0.06 (±0.00)
	Stem	0.02 (±0.00)	0.01 (±0.00)	0.03 (±0.00)
	Root	0.02 (±0.00)	0.08 (±0.00)	0.03 (±0.00)
	Soil	0.01 (±0.00)	0.01 (±0.00)	0.01 (±0.00)
Level 2	Leaf	0.34 (±0.01)	0.14 (±0.00)	0.10 (±0.00)
	Stem	0.09 (±0.00)	0.05 (±0.00)	0.12 (±0.00)
	Root	0.23 (±0.00)	0.14 (±0.00)	0.13 (±0.00)
	Soil	0.72 (±0.01)	1.66 (±0.03)	0.53 (±0.01)
Level 3	Leaf	1.83 (±0.03)	0.58 (±0.01)	0.34 (±0.01)
	Stem	1.60 (±0.03)	0.68 (±0.01)	0.28 (±0.01)
	Root	0.88 (±0.02)	0.80 (±0.01)	0.82 (±0.02)
	Soil	2.35 (±0.04)	1.97 (±0.04)	2.44 (±0.06)

LOD, limit of detection.

This high Ni accumulation efficiency is in agreement with the literature [29]. Based on the toxic effects observed on the plant phenotype after day 14, strong hyperaccumulation could lead to the observed dieback of *A. murale* (level 3). Compared to Tappero et al., the Ni hyperaccumulation (0.16%) was very effective using dissolved metal species. In the case of Co, the accumulated metal was more uniformly distributed in the different plant tissues and was generally lower in concentration (Table 1, blue). Hence, a reduced translocation velocity can be assumed. Nevertheless, Co-contaminated plants showed the same phenotypical intoxication effects after day 14, indicating a higher Ni tolerance of *A. murale* compared to Co (e.g., via effective vacuolar sequestration) [19]. Mn was quantified to 0.02 wt% in the leaves and the soil of the control group due to its natural abundance (Table 1, grey). It was not observed in stems or roots. Hence, the sequestration of Mn is located in the leaves of *A. murale* (or high expression of Mn-containing proteins). In contrast to Ni and Co, the hyperaccumulation process was slower and a high concentration was only detected in the roots after a short accumulation phase (Table 1, red). Concentrations in soils showed high variations, which can be ascribed to an inhomogeneous distribution, particularly due to crystallization at levels 2 and 3, as well as difficulties regarding the sampling process without harming the plants.

Different concentrations in plant tissues and transition metals can be explained via varying transporter selectivity, translocation velocity (complexation affinity), sequestration mechanisms, and storage locations. To visualize the lateral distribution of transition metals in *A. murale* leaves, micro X-ray fluorescence spectroscopy (μ XRF) measurements were performed (Figure 1). The monitored lateral distribution of transition metals is discussed via implementation of information from the literature. The transition metal uptake in *A. murale* leaves revealed different lateral distributions. Images of the leaves at contamination levels 1 and 2 for Ni, Co, and Mn after the accumulation phase are shown in the supporting information (Figure S4).

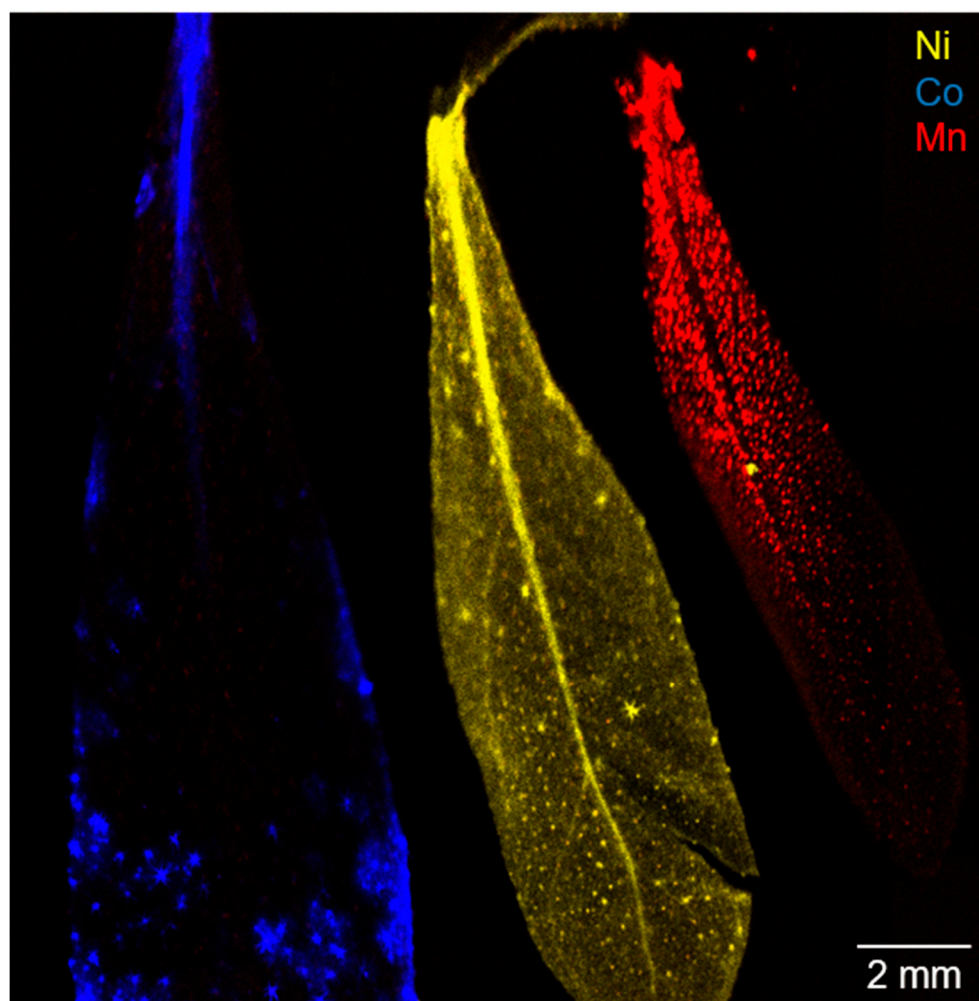


Figure 1. Micro X-ray fluorescence spectroscopy (μ XRF) image of three *alyssum murale* leaves from the highest contamination group (level 3). Co localization is indicated in blue, Ni in yellow, and Mn in red.

The Ni uptake mechanism was studied intensively in recent years and the translocation can be described by multiple complexation and decomplexation steps (chelating agents like histidine, glutamine, and carboxylic acids) during the Ni^{2+} transport from the roots via the xylem to the leaf [21]. In the leaf, Ni is generally complexed by citric acid and sequestered in leaf vacuoles via transporters from the zinc transporter protein (ZIP) family [21]. Hence, a dot-shaped accumulation was observed for low concentrations (Figure S4 level 1 and 2, Figure 4). With increasing Ni concentrations in the leaf (i.e., level 3), palisade mesophyll and apoplast become an important storage compartment, and this is in agreement with the homogenous, smooth lateral distribution in the μ XRF image (Figure 1) [36]. Consequently, the sequestration of Ni^{2+} in multiple leaf tissues culminates in a more homogenous accumulation, and the signals highlight the overall structure of the leaf (e.g., leaf-veins). Furthermore,

a trend from leaf tip to increasing leaf bulk sequestration can be concluded with increasing Ni concentrations (Figure S4).

Co was accumulated in the leaf apex and leaf margins with strong local accumulation effects and, presumably, a co-localization with Ca-rich trichomes on the surface of the leaf (Figure S3). This observation was present for all three concentration levels. Therefore, a selective excretion mechanism for Co that gets translocated to the leaf surface by guttation fluids possibly via assistance of trichomes can be assumed (see Figures S2–S4) [19]. Ultimately, the sequestration mechanism for Co was also observed in the form of a Co-rich mineral precipitate on the leaf surface (Figure S2, red-colored trichomes) [37]. The obtained findings regarding the Ni and Co localization in the leaf are fully consistent with Tappero et al. [19].

Mn showed dot-shaped areas with increased intensity from the stem to leaf tip and a negative image of the central leaf-vein for all three concentration levels. In particular, Mn contamination levels 1 and 2 resulted in a comparable distribution image to the Ni hyperaccumulation (Figure S4). Consequently, for Mn sequestration, a distinct association with specific storage organs can be assumed, and it likely differs solely for high concentrations from the Ni sequestration mechanism (Figure 1 and Figure S4). In light of LIB transition metal phytoremediation, the possibly higher selectivity and larger total accumulation of valuable and toxic Ni and Co compared to Mn are advantageous. In the present watering study with dissolved metal species, the metal sequestration mechanism of *alyssum murale* differs distinctly for Ni, Co, and Mn, as well as for varying concentration levels, supporting the varying selectivity and efficiency concluded from Table 1.

After the contamination process, the same plants were watered in an accumulation phase with deionized water, and the three specific plant tissues (leaf, stem, root) were harvested after a further 26 days. In order to prove the transition metal uptake dependency on an active transport mechanism instead of passive diffusion, the concentrations of the contamination and accumulation phase are compared in Table 2. All leaf samples showed increased Ni, Co, and Mn concentrations after 26 days of accumulation (>20%). Hence, leaves are likely the main storage organ for Ni, Co, and Mn hyperaccumulation [21]. Overall, a distinct trend for accumulation in plant tissues, especially for higher concentrations (18/27, green), and a reduced contamination of soils were observed (7/9, red). For contamination levels 1 and 2, all plants were vital over the whole experiment time. Overall, the translocation factors (leaf to root ratio) for the three metals were in the range of 1–3, which is in good agreement with the literature [19]. The Co accumulation exceeded that of Ni, highlighting the capabilities of *A. murale* for possible application in the LIB context, which is accordance with literature findings [19]. For the lowest contamination level, a low accumulation in stems and roots was detected. Therefore, an effective transport for all transition metals through the plant into leaves in vital plants can be assumed for lowly concentrated metals. The reduced translocation for Mn monitored in the contamination phase was confirmed in the accumulation phase. High concentrations in roots and stems for all plants exposed to level 3 can be presumably ascribed to a “snapshot” of the dieback-associated interruption of the metabolism. Nonetheless, soil concentrations decreased even after the first observation of phytotoxicity in *A. murale* during the contamination phase. Consequently, the accumulation process is possibly uncontrolled, and no saturation effects were observed. Finally, hyperaccumulation of *A. murale* for this short exposition time was limited to $\approx 2\text{--}3$ wt% of Ni/Co due to the arising dieback of plants.

Table 2. Quantified concentrations of Ni, Co, and Mn in wt% by means of ICP-OES regarding dry matter of *alyssum murale* and dried soil after 20 days of contamination (con) and 26 further days of accumulation (acc). Measurable accumulation in plant tissues is highlighted in green, highest values in bold, and remediation of soils in red (n = 3).

Contamination Group	Sample	Ni _{con} /wt%	Ni _{acc} /wt%	Co _{con} /wt%	Co _{acc} /wt%	Mn _{con} /wt%	Mn _{acc} /wt%
Control	Leaf	<LOD	<LOD	<LOD	<LOD	0.02 (±0.00)	0.01 (±0.00)
	Stem	<LOD	<LOD	<LOD	<LOD	<LOD	<LOD
	Root	<LOD	<LOD	<LOD	<LOD	<LOD	<LOD
	Soil	<LOD	<LOD	<LOD	<LOD	0.02 (±0.00)	0.02 (±0.00)
Level 1	Leaf	0.04 (±0.00)	0.09 (±0.00)	0.06 (±0.00)	0.15 (±0.00)	0.06 (±0.00)	0.10 (±0.00)
	Stem	0.02 (±0.00)	0.02 (±0.00)	0.01 (±0.00)	0.01 (±0.00)	0.03 (±0.00)	0.02 (±0.00)
	Root	0.02 (±0.00)	0.02 (±0.00)	0.08 (±0.00)	0.01 (±0.00)	0.03 (±0.00)	0.02 (±0.00)
	Soil	0.53 (±0.00)	0.31 (±0.01)	0.50 (±0.01)	0.28 (±0.01)	0.29 (±0.01)	0.35 (±0.01)
Level 2	Leaf	0.34 (±0.01)	0.40 (±0.01)	0.14 (±0.00)	0.49 (±0.01)	0.10 (±0.00)	0.28 (±0.01)
	Stem	0.02 (±0.00)	0.08 (±0.00)	0.05 (±0.00)	0.13 (±0.00)	0.12 (±0.00)	0.11 (±0.00)
	Root	0.23 (±0.00)	0.15 (±0.00)	0.14 (±0.00)	0.31 (±0.01)	0.13 (±0.00)	0.10 (±0.00)
	Soil	2.97 (±0.05)	2.50 (±0.04)	1.23 (±0.02)	1.30 (±0.02)	1.16 (±0.03)	1.07 (±0.03)
Level 3	Leaf	1.83 (±0.03)	2.19 (±0.04)	0.58 (±0.01)	0.66 (±0.01)	0.34 (±0.01)	0.41 (±0.01)
	Stem	1.60 (±0.03)	3.22 (±0.06)	0.68 (±0.01)	1.97 (±0.04)	0.28 (±0.01)	0.61 (±0.02)
	Root	0.88 (±0.02)	1.20 (±0.02)	0.80 (±0.01)	2.53 (±0.05)	0.82 (±0.02)	1.50 (±0.04)
	Soil	3.11 (±0.05)	2.72 (±0.05)	2.62 (±0.05)	2.34 (±0.04)	3.11 (±0.08)	2.72 (±0.07)

Contamination, con; accumulation, acc; LOD, limit of detection.

2.2. Phytoremediation of Battery Materials—Proof-of-Concept

In a successive approach, the uptake behavior from actual battery materials in the form of a cathode material (NCM111) was evaluated. As the soil extraction mechanism of *A. murale* is still not fully understood, the bioavailability is presumably related to the dissolved metal cations. Therefore, aqueous solutions with varying pH values were mixed with battery ash from a 5 Ah pouch cell after the deactivation. The metal contents were measured to be 3.76 wt% Li, 11.81 wt% Ni, 11.84 wt% Co, and 11.23 wt% Mn. Experiments revealed a slow dissolution, as well as a strong pH dependency for transition metals (see Figure 2). Overall, the transition metal dissolution was <20% for natural tolerable pH values (pH 3–8), whereby Ni showed the highest yields after three weeks (17.4%) though only limited dissolution (or reprecipitation) for pH 6 and 8. Lithium showed a comparable fast and constant dissolution of ≈20% for all pH values, stagnating for pH 5, 6, and 8. At pH 3 and 4, yields of 48.6–68.0% were achieved after 21 days.

Consequently, the conversion of NCM111 to dissolved metal cations by acidifying the soil can possibly improve the bioavailability and the uptake efficiency of *A. murale* (e.g., acid rain, presence of lead–acid batteries in landfills) [38]. The proof-of-concept study was conducted at a natural soil pH of ≈6 without acidic modifier addition. Furthermore, pristine NCM-oxide particles were used to examine the accumulation capabilities under realistic conditions comparable to LIB contamination at repositories/landfill sites. Adult *A. murale* plants were exposed to metalliferous soil directly after the mixing of soil with NCM111. The natural NCM111 degradation and transition metal dissolution initiated parallel to the beginning of the study and was presumably <5% over the entire exposition time (see Figure 2, pH 6). After 100 days, plants were harvested, and plant tissues were investigated by means of ICP-OES and μ XRF analogously to Section 2.1. Considering the natural rain pH value, as well as a decreased soil pH value due to mixed battery waste (e.g., lead–acid batteries), the bioavailability of metal species can be distinctly higher.

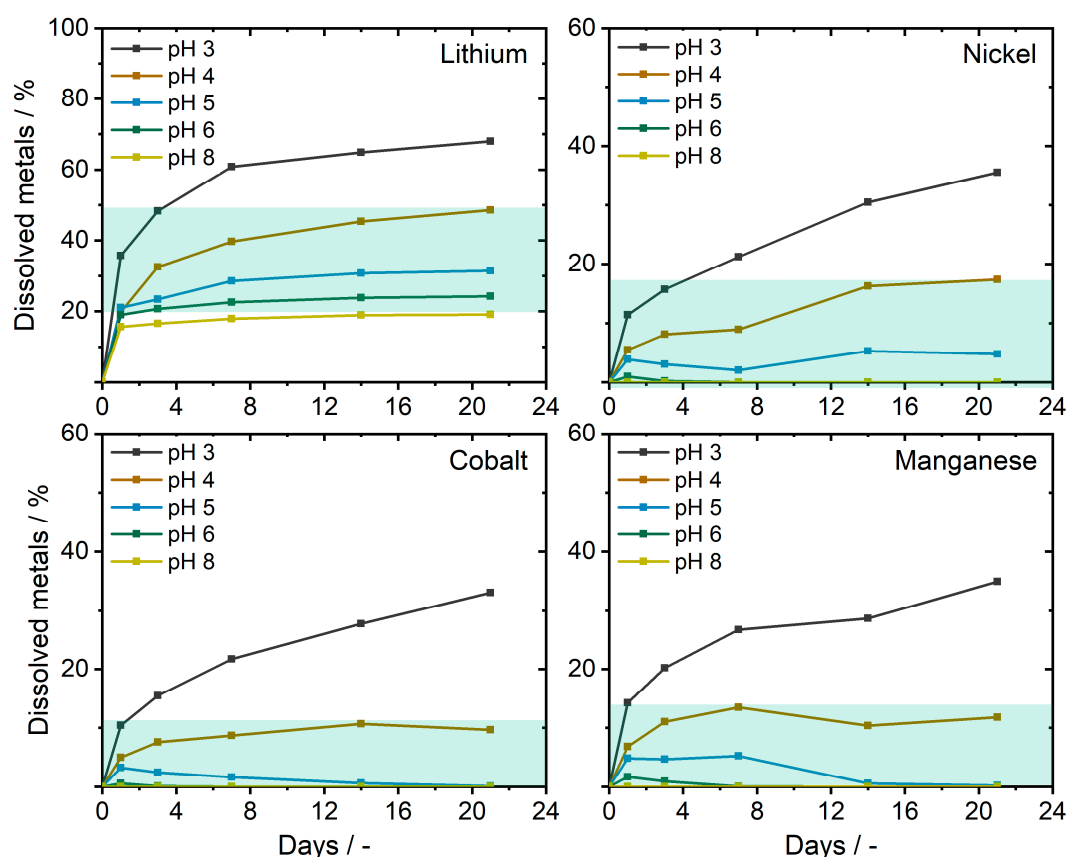


Figure 2. Lithium-ion batteries (LIB) metal dissolution from the ash of deactivated pouch cells (NCM111 positive electrode material) in aqueous media at different pH values. Values observed at an acceptable soil pH range for plants are indicated in green (pH 3–8).

LA-ICP-MS was conducted to improve the imaging sensitivity and to access the lateral distribution of Li. Metal concentrations quantified via ICP-OES are summarized in Table 3. The completeness of the mixing process of NCM111 (40.0 g) and soil (8.0 kg) was checked by four samples and revealed adequate relative standard deviations (<10%) and good accordance of calculated and measured values (see Table 3). At the end of the study, four soil samples were collected after plant harvesting and mixing of the remaining soil. The distinctly reduced soil concentration can more likely be ascribed to an agglomeration of particles due to the flushing effect during the watering process than accumulation in plant compartments. Flushing of the empty plastic sample tub with nitric acid also revealed low transition metal concentrations. Consequently, a strong local agglomeration of NCM111 particles in the soil represents the proposed effect for this observation. Nonetheless, all metals were detected in the leaves of *A. murale* despite the short exposition time. Assuming a bioavailability only for dissolved species, the transition metal quantified <math><1 \text{ mg kg}^{-1}</math> is in accordance with the low concentrations applied, slow and low dissolution (<5%), as well as the short exposure time (Table 3). Higher concentrations of Li in all plant tissues are consistent with the results of the dissolution experiments. The proof-of-concept in terms of the phytoextraction of LIB-related metals from intact electrode material was, therefore, successful.

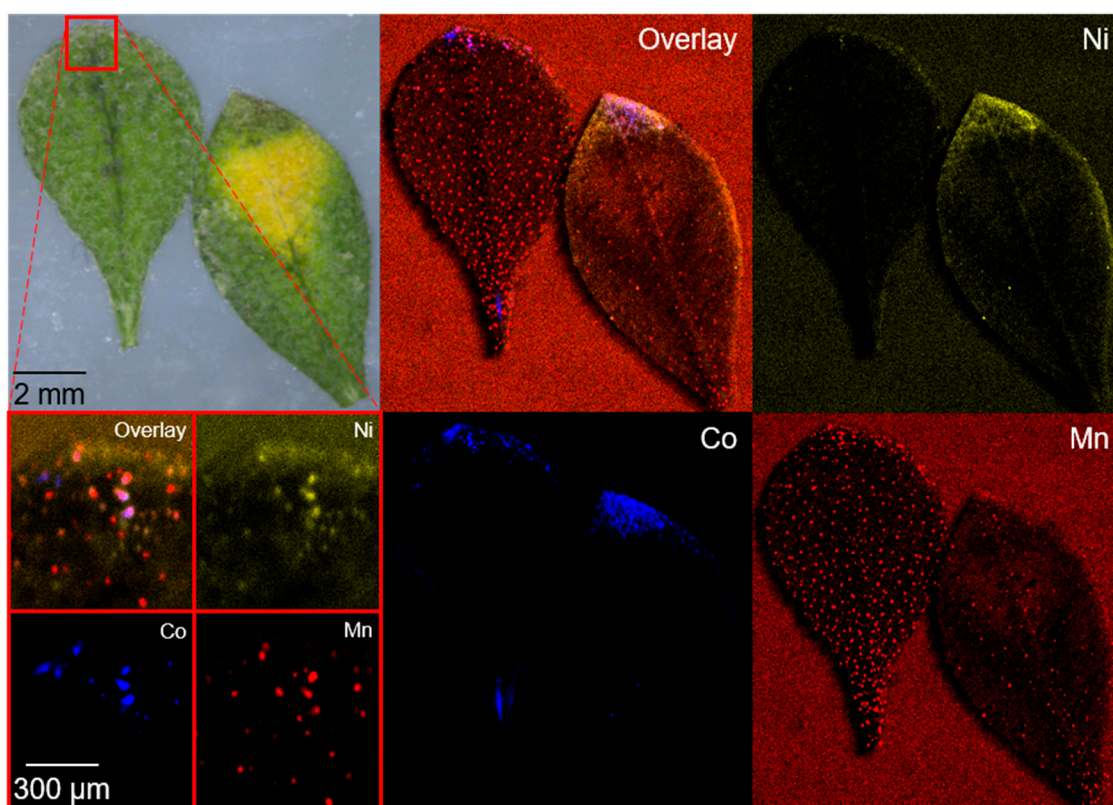


Figure 3. Microscopic and μ XRF images of two *A. murale* leaves, as well as a small section (red square) from the leaf tip after 100 days of NCM111 soil contamination. Co localization is indicated in blue, Ni in yellow, and Mn in red. A dot-shaped distribution was observed for all metals (see small section) and a localization in the tip of the leaves can be seen for Ni and Co.

Table 3. Quantified concentrations of Ni, Co, Mn, and Li in mg L^{-1} by means of ICP-OES regarding dry matter of *A. murale* and dried soil after 100 days of NCM111 contamination ($n = 3$).

Contamination Group	Sample	Ni/ mg kg^{-1}	Co/ mg kg^{-1}	Mn/ mg kg^{-1}	Li/ mg kg^{-1}
Soil contamination Start	Calculated	1449 (± 25)	1455 (± 27)	1356 (± 35)	514 (± 12)
	Measured	1975 (± 34)	1925 (± 35)	2150 (± 55)	575 (± 14)
After 100 days	Measured	2.73 (± 0.05)	2.69 (± 0.05)	2.69 (± 0.07)	0.91 (± 0.02)
<i>Alyssum murale</i> after 100 days	Leaf	0.49 (± 0.01)	0.63 (± 0.01)	0.78 (± 0.02)	5.90 (± 0.14)
	Stem	<LOD	<LOD	0.30 (± 0.01)	0.30 (± 0.01)
	Root	<LOD	<LOD	<LOD	0.32 (± 0.01)

LOD, limit of detection.

The accumulation of lowly concentrated transition metals in leaves showed a dot-shaped localization in the tip of the leaves with co-localization and differs from the accumulation behavior for high concentrations in Section 2.1 (Figures 1 and 3, and Figure S4). Sequestration in the leaf apex and leaf margin for low concentrations of Ni and Co was observed, and these findings are in accordance with the literature [21,39].

The lateral distribution of Li was investigated by means of LA-ICP-MS, and a co-localization of transition metals observed with μ XRF was confirmed (see Figure 3, white areas). Three ablation runs were conducted to obtain more depth information. Li (top row) and the overlay of transition metals (bottom row) after the first (top layer) and third ablation run (deeper layer) are shown in Figure 4. The small Li cation is apparently distributed in the whole leaf and presumably present in the cytosol and water-bearing tissues (xylem/phloem). This assumption is based on the finding of reduced Li signals in parched leaf areas (see Figure S5). Considering the low concentrations of transition metals,

the assumption of effective vacuolar sequestration of Ni and Co, and hence, no co-localization with trichome structures is consistent with the literature [19]. Overall, the accumulation of toxic transition metals in the leaf tip is consistent with the interpretation of hyperaccumulation as an elemental-defense strategy of *A. murale*.

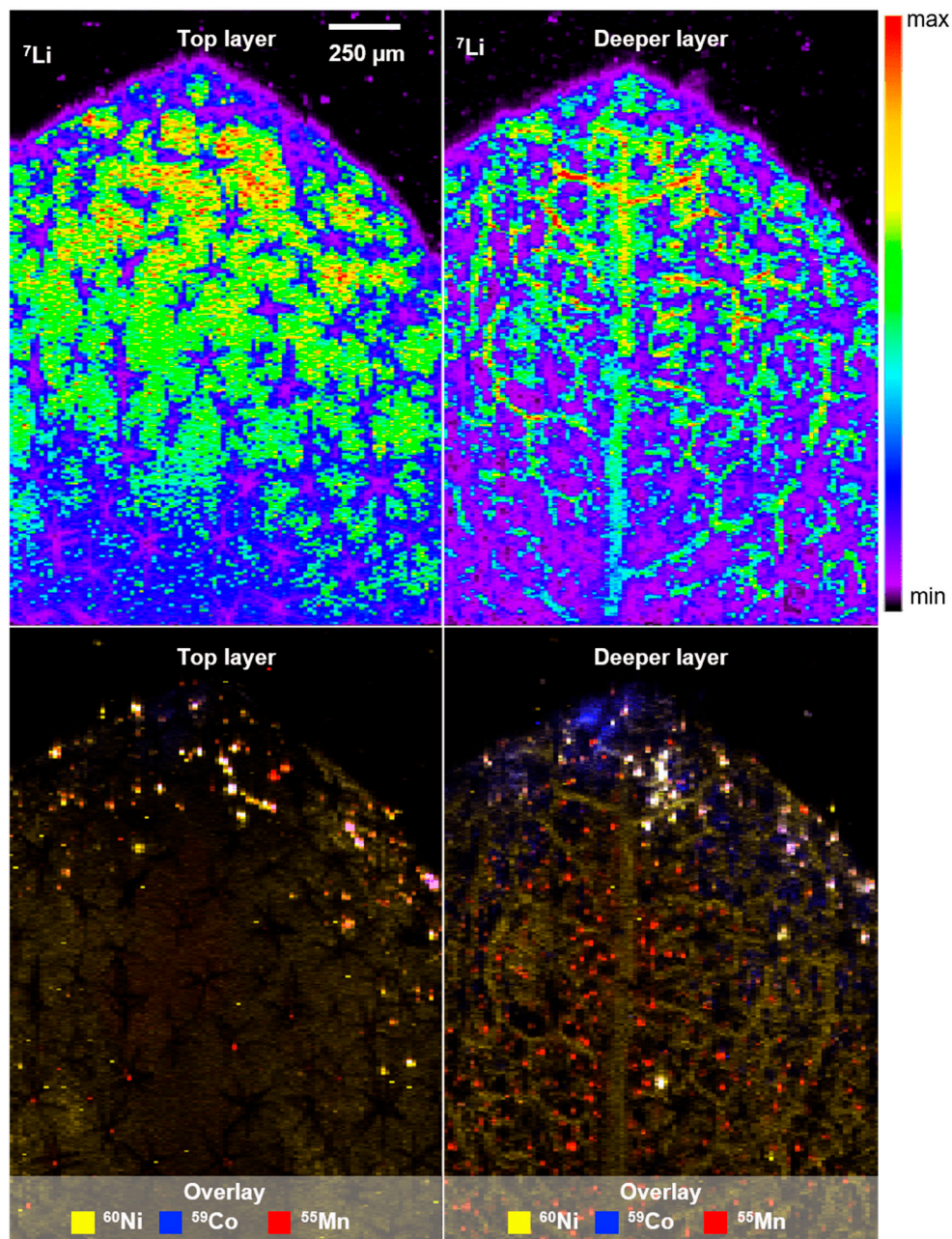


Figure 4. LA-ICP-MS image showing the Li distribution in the surface layer and deeper mesophyll (top), as well as the respective overlay of transition metal distribution (Ni, Co, Mn; bottom) in a leaf of *alyssum murale*. Co-localization of transition metals is shown in white.

After long-term exposure of LIB materials to the environment, the accessible metal content will be distinctly higher, and the bioavailability increased by mild acidification of the metalliferous soil or the translocation can be improved via chelating agents [40]. Furthermore, by means of seeding experiments (higher biomass growth compared to adult plants), as well as a longer

accumulation period, *alyssum murale* can be used for phytoremediation approaches for LIB metals from repositories/landfill sites.

3. Materials and Methods

For chemicals and materials applied in this work, as well as detailed instrumental parameters of the respective devices, the reader is kindly referred to the supporting information.

3.1. Contamination Studies with *Alyssum Murale*

Accumulation of Ni, Co, and Mn from Irrigation Water

A contamination study based on dissolved transition metals in irrigation water was conducted with 40 plants of the species *A. murale*. Plant material was obtained from Staudengärtnerei Tangermann (Nordstemmen, Germany). Plants were about one year old (height about 5 cm), grown in standard soil in flower pots of 1 L content. Cultivation was performed from April to August 2019 in a cold greenhouse area (average temperature 20 °C; 51°58′10.1″N, 7°35′54.3″E). Three concentration levels 1–3 (0.2, 1.0, and 5.0 g L⁻¹) using one of the respective transition metals (Ni, Co, Mn) were prepared in distilled water (detailed information can be found in the supporting information). Hence, nine different contamination groups with four plants each were watered with the respective metal/concentration-combinations every second day for 20 days (see Table 4). Simultaneously, four plants were watered with distilled water as the control group. The quantity of irrigation water was set to 50 mL per watering for 46 days and added in a stepwise procedure to consider the capacity of the soil and prevent flushing of metals. Sampling was conducted after day 20 (contamination phase) and day 46 (accumulation phase). Between day 20 and 46, the plants were watered with distilled water.

Table 4. Added transition metal cation content (Ni²⁺, Co²⁺, Mn²⁺) in the respective irrigation water groups during a contamination time of 20 days. The total contamination of the respective transition metal for one plant was 0.1, 0.5, and 2.5 g.

Transition Metal	Contamination Day											
	Addition	0.	2.	4.	6.	8.	10.	12.	14.	16.	18.	20.
∑ Level 1/g	0.00	0.01	0.02	0.03	0.04	0.05	0.06	0.07	0.08	0.09	0.10	
∑ Level 2/g	0.00	0.05	0.10	0.15	0.20	0.25	0.30	0.35	0.40	0.45	0.50	
∑ Level 3/g	0.00	0.25	0.50	0.75	1.00	1.25	1.50	1.75	2.00	2.25	2.50	

3.2. Electrode Material Dissolution

Metal dissolution experiments of LIB ash (2.0 g) from deactivated 5 Ah pouch cells (thermal deactivation for 20 min and ≈ 300 °C) were performed in aqueous media (50 mL). Due to the highly basic nature of the solution, the pH was adjusted to 3.5, 4.0, 5.0, 6.0, and 8.0 with acetic acid. Aliquots of the sample (200 μL) were used for inductively coupled plasma-optical emission spectroscopy (ICP-OES) after centrifugation (8500 rpm, 10 min) at day 1, 3, 7, 14, and 21.

Li, Ni, Co, and Mn Accumulation from Electrode Material

An electrode material contamination of the soil was conducted by using NCM111 particles. The electrode material (40.0 g, an equivalent of a 5 Ah pouch cell, ≈ 2.88 g Li, 8.13 g Ni, 8.16 g Co, 7.61 g Mn) was added stepwise to 8.0 kg of soil (≈ 30% soil humidity, corresponds to ≈ 5.6 kg dry soil) during constant homogenization. The soil contamination was calculated to 0.51 g kg⁻¹ Li, 1.45 g kg⁻¹ Ni, 1.46 g kg⁻¹ Co, and 1.36 g kg⁻¹ Mn after drying. Adult *A. murale* plants (15) were ingrafted, placed in a conservatory, and allowed to accumulate transition metals over a time of 100 days between August and November 2019 (51°58′10.1″ N, 7°35′54.3″ E). Accumulation studies in sections were conducted under exclusion of rainwater to prevent the flushing of metals and waterlogging.

3.3. Inductively Coupled Plasma-Optical Emission Spectroscopy

Leaves, stems, and roots were collected uniformly from all plants of the respective watering contamination groups and within the electrode material contamination group. Soil samples were investigated after homogenization and drying (72 h, 80 °C) to overcome possible crystallization and sedimentation effects of metals. Roots of *A. murale* were washed with water for 2 min to remove inherent soil. Furthermore, leaves and stems of the watering contamination groups were washed to exclude the possibility of splash water contamination (Figure 5). ICP-OES sample preparation comprised (i) manual cutting of the stems/roots, (ii) liquid nitrogen freezing and homogenization in a mortar, (iii) drying at 80 °C for 72 h, and (iv) sample weighing for the subsequent microwave digestion based on Diehl et al. (see Figure 1) [41].

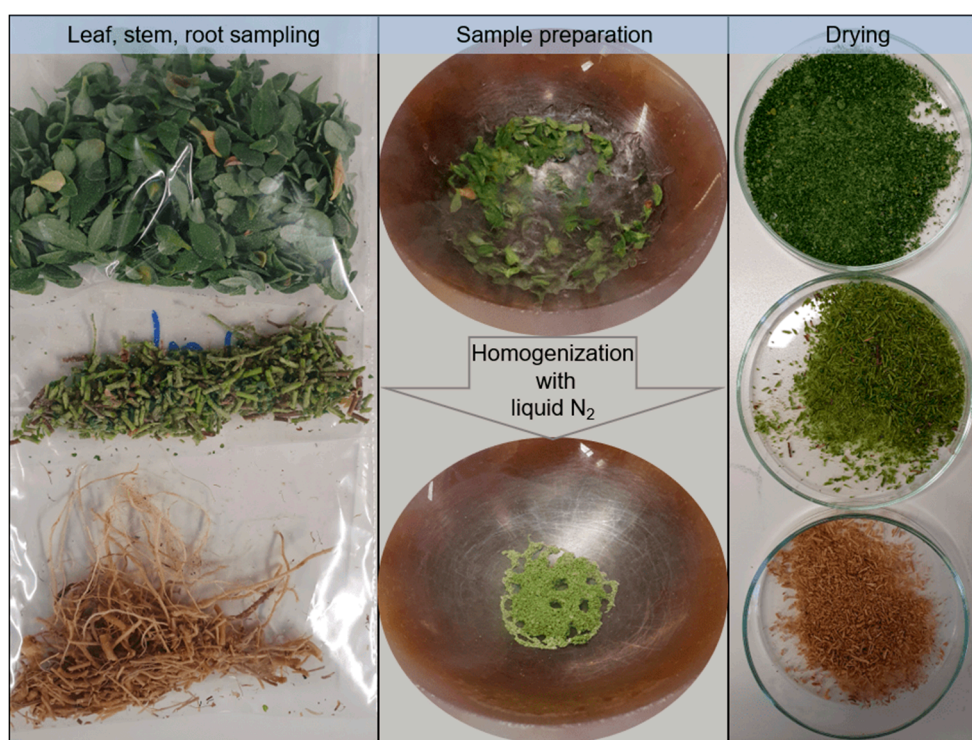


Figure 5. Sample preparation workflow of leaves, stems, and roots of *A. murale* prior to microwave digestion for ICP-OES measurements. The homogenization of leaves is shown exemplarily.

3.3.1. Micro X-ray Fluorescence Spectroscopy

The distribution of the transition metals in the leaves was monitored by means of micro X-ray fluorescence spectroscopy (μ XRF). Leaf samples were flushed with deionized water and pressed between microscope slides for 24 h. A M4 Tornado (Bruker, Bruker Nano GmbH, Berlin, Germany) with a Rh source was used and operated at 50 kV and 600 μ A. The measurements were conducted at atmospheric pressure with a dwell time of 10 ms and 29 μ m spot size with a 20 μ m distance between each spot (Figure 1). The images were recorded five times and averaged. Conditions were varied for three repetitions with a measurement time of 26 ms and 29 μ m spot size with a 20 μ m distance between each spot (Figure 3). The small section was measured for four times with a measurement time of 100 ms and 29 μ m spot size with a 5 μ m distance between each spot. The emitted X-ray fluorescence was detected using a silicon drift detector (SDD, XFlash[®] 5030, Bruker). Data evaluation and image processing were carried out using the software ESPRIT HyperMap (Bruker).

An ICP-OES system (ARCOS, Spectro Analytical Instruments, Kleve, Germany) with axial plasma viewing and a standard Fassel-type torch (i.d. 1.8 mm) was used for elemental determination. For sample introduction, the system's peristaltic pump with a cross-flow nebulizer and a double-pass

spray chamber (Scott type) was used. Element emission was detected at different individual emission lines simultaneously, and quantification was conducted via external calibration. The standard deviation of measurements was <5% for all measured samples. All samples were measured three times with an integration time of 28 s. Detailed operation and measurement conditions are shown in the supporting information (Table S1).

3.3.2. Laser Ablation-Inductively Coupled Plasma-Mass Spectrometry

For determination of low concentrations of transition metals and lithium, as well as their lateral distribution in leaves, laser ablation-inductively coupled plasma-mass spectrometry (LA-ICP-MS) was performed. Samples were pressed between microscope slides for 24 h prior to measurements. Afterward, samples were ablated with a LSX-213 LA unit (Teledyne Technologies, Thousand Oaks, CA, USA) using a 213 nm-frequency quintupled Q-switched Nd:YAG laser with a pulse length of <6 ns and a maximum source pulse energy of >4 mJ. The sample surface was scanned by successive line scans of the pulsed laser. The ablated material was transported by a constant He gas flow to a 7700x-Series ICP-MS (Agilent Technologies, Santa Clara, CA, USA) for elemental detection. Line scans were recorded as transient measurements and translated to elemental mappings afterward by the software ImaJar. Varying ablation efficiencies were corrected by normalizing the measured elemental signals to the ^{13}C signal. Detailed instrumental parameters are given in the supporting information (Table S2) [42].

4. Conclusions

The phytoremediation capabilities of *A. murale* regarding commonly applied metals and constituents in lithium-ion battery cells were examined in this study. A contamination approach with the dissolved transition metals Ni, Co, and Mn in irrigation water showed translocation and hyperaccumulation for all metals up to 3 wt% in the dry matter of different plant tissues (leaf, stem, root). In the following accumulation phase, metal concentrations in all plant compartments increased significantly (leaves > 20%) and soil concentrations decreased (10–50%), proving the active uptake of Ni, Co, and Mn in *alyssum murale* and its phytoremediation capabilities. The sequestration was monitored via μXRF measurements and revealed a homogenous distribution of Ni in the leaf for high concentrations (multicompartment sequestration), and culmination in the leaf apex for reduced contamination and single-compartment storage (e.g., vacuolar sequestration). For Mn, a dot-shaped localization was observed, which can be ascribed to a sequestration mechanism based on specific cell compartments independent from the contamination degree. The hyperaccumulation of Co showed a distinct local concentration in the leaf apex and margins, resulting in chlorosis and the drying-up of the leaf area. Consequently, different processes for the translocation and sequestration could be shown for all investigated metals with promising accumulation quantities for the valuable metals Ni and Co.

In the second part of the study, hyperaccumulation was investigated under realistic conditions in terms of administered concentrations, bioavailability (stability and dissolution behavior of intact NCM111 layered oxide at varying pH), and accumulation time (100 days). Furthermore, Li was added to the monitored elements and LA-ICP-MS measurements were performed for the lateral and depth distribution in the leaf. Li was homogeneously distributed over the whole leaf, and the deeper layers indicated its presence in water-bearing areas (xylem/phloem) areas, as well as a translocation mechanism based on a passive diffusion instead of active accumulation. The accumulation of all transition metals (<1 mg kg⁻¹) and Li (6 mg kg⁻¹) confirmed the proof-of-concept approach of this study using phytoremediation in the context of lithium-ion battery materials. In light of insufficient recycling loops for LIBs and the significant sales figures in recent years, phytoremediation of commonly applied metals can occupy a valuable niche to recover costly Ni and Co wastes back into the production process and enhance sustainability. In particular, the use of this low-cost and green technology at repositories/landfill sites or disused mines with low environmental standards possesses the potential to reduce the overall ecological damage accompanied by the enormous success of LIBs.

Supplementary Materials: The following are available online at <http://www.mdpi.com/2313-4321/5/4/26/s1>.

Author Contributions: J.H. had the idea and performed the experiments, which is not stated elsewhere. M.M. and P.H. performed the LA-ICP-MS measurements, while M.D. performed the soil analysis by ICP-OES. J.B. and F.K. were supervised by J.H., S.N. and M.W. during their bachelor theses that they carried out on this topic. L.S. and U.K. were responsible for the μ XRF measurements and A.H. helped with all points regarding the plant mechanisms. S.N. is the head and principal investigator of the work of J.H., and M.W. is the head of the institute. All authors have read and agreed to the published version of the manuscript.

Funding: The authors acknowledge the German Federal Ministry of Education and Research for funding the project “Cell-Fi” (03XP0069B).

Acknowledgments: Special thanks to Lars Krüger and colleagues from the Institute for Pharmaceutical Biology and Phytochemistry (IPBP, WWU Münster) for supporting the experimental executions.

Conflicts of Interest: The authors declare no conflict of interest.

References

1. Winter, M.; Barnett, B.; Xu, K. Before Li Ion Batteries. *Chem. Rev.* **2018**, *23*, 11433–11456. [[CrossRef](#)] [[PubMed](#)]
2. Placke, T.; Kloepsch, R.; Dühnen, S.; Winter, M. Lithium Ion, Lithium Metal, and Alternative Rechargeable Battery Technologies: The Odyssey for High Energy Density. *J. Solid State Electrochem.* **2017**, *21*, 1939–1964. [[CrossRef](#)]
3. Betz, J.; Bieker, G.; Meister, P.; Placke, T.; Winter, M.; Schmich, R. Theoretical versus Practical Energy: A Plea for More Transparency in the Energy Calculation of Different Rechargeable Battery Systems. *Adv. Energy Mater.* **2019**, *9*, 1–18. [[CrossRef](#)]
4. Christophe Pillot. The Rechargeable Battery Market and Main Trends 2018–2030. In Proceedings of the Advanced Automotive Battery Conference, San Diego, CA, USA, 24 May 2019.
5. Schmich, R.; Wagner, R.; Hörpel, G.; Placke, T.; Winter, M. Performance and Cost of Materials for Lithium-Based Rechargeable Automotive Batteries. *Nat. Energy* **2018**, *3*, 267–278. [[CrossRef](#)]
6. Rothermel, S.; Krueger, S.; Winter, M.; Nowak, S. Hydrometallurgical Processing and Thermal Treatment of Active Materials. In *Recycling of Lithium-Ion Batteries*; Springer International Publishing: Basel, Swiss, 2018; pp. 219–246.
7. Diekmann, J.; Gruetzke, M.; Loellhoeffel, T.; Petermann, M.; Rothermel, S.; Winter, M.; Nowak, S.; Kwade, A. Recycling of Lithium Ion Batteries—Reapplication of the Recovered Materials as Lithium Ion Battery Materials. In *Recycling of Lithium-Ion Batteries*; Springer International Publishing: Basel, Swiss, 2018; pp. 39–51.
8. Nowak, S.; Winter, M. The Role of Sub- and Supercritical CO₂ as “Processing Solvent” for the Recycling and Sample Preparation of Lithium Ion Battery Electrolytes. *Molecules* **2017**, *22*, 403. [[CrossRef](#)]
9. Rothermel, S.; Evertz, M.; Kasnascheetw, J.; Qi, X.; Grütze, M.; Winter, M.; Nowak, S. Graphite Recycling from Spent Lithium Ion Batteries Graphite Recycling from Spent Lithium Ion Batteries. *ChemSusChem* **2016**, *9*, 3473–3484. [[CrossRef](#)]
10. Diekmann, J.; Rothermel, S.; Nowak, S.; Kwade, A. The LithoRec Process. In *Recycling of Lithium-Ion Batteries*; Springer International Publishing: Basel, Swiss, 2018; pp. 33–38.
11. Krüger, S.; Hanisch, C.; Kwade, A.; Winter, M.; Nowak, S. Effect of Impurities Caused by a Recycling Process on the Electrochemical Performance of Li[Ni_{0.33}Co_{0.33}Mn_{0.33}]O₂. *J. Electroanal. Chem.* **2014**, *726*, 91–96. [[CrossRef](#)]
12. Erickson, E.M.; Schipper, F.; Penki, T.R.; Shin, J.-Y.; Erk, C.; Chesneau, F.-F.F.; Markovsky, B.; Aurbach, D. Review—Recent Advances and Remaining Challenges for Lithium Ion Battery Cathodes. *J. Electrochem. Soc.* **2017**, *164*, A6341–A6348. [[CrossRef](#)]
13. Schipper, F.; Erickson, E.M.; Erk, C.; Shin, J.-Y.; Chesneau, F.F.; Aurbach, D. Review—Recent Advances and Remaining Challenges for Lithium Ion Battery Cathodes. *J. Electrochem. Soc.* **2017**, *164*, A6220–A6228. [[CrossRef](#)]
14. Watari, T.; McLellan, B.C.; Giurco, D.; Dominish, E.; Yamasue, E.; Nansai, K. Total Material Requirement for the Global Energy Transition to 2050: A Focus on Transport and Electricity. *Resour. Conserv. Recycl.* **2019**, *148*, 91–103. [[CrossRef](#)]
15. Cappa, J.J.; Pilon-Smits, E.A.H. Evolutionary Aspects of Elemental Hyperaccumulation. *Planta* **2014**, *239*, 267–275. [[CrossRef](#)]

16. Pollard, A.J.; Reeves, R.D.; Baker, A.J.M. Facultative Hyperaccumulation of Heavy Metals and Metalloids. *Plant Sci.* **2014**, *217–218*, 8–17. [[CrossRef](#)]
17. Rascio, N.; Navari-Izzo, F. Heavy Metal Hyperaccumulating Plants: How and Why Do They Do It? And What Makes Them so Interesting? *Plant Sci.* **2011**, *180*, 169–181. [[CrossRef](#)] [[PubMed](#)]
18. Krämer, U. Metal Hyperaccumulation in Plants. *Annu. Rev. Plant Biol.* **2010**, *61*, 517–534. [[CrossRef](#)] [[PubMed](#)]
19. Tappero, R.; Peltier, E.; Gräfe, M.; Heidel, K.; Ginder-Vogel, M.; Livi, K.J.T.; Rivers, M.L.; Marcus, M.A.; Chaney, R.L.; Sparks, D.L. Hyperaccumulator *Alyssum Murale* Relies on a Different Metal Storage Mechanism for Cobalt than for Nickel. *New Phytol.* **2007**, *175*, 641–654. [[CrossRef](#)] [[PubMed](#)]
20. Liu, K.; Yu, F.; Chen, M.; Zhou, Z.; Chen, C.; Li, M.S.; Zhu, J. A Newly Found Manganese Hyperaccumulator—*Polygonum Lapathifolium* Linn. *Int. J. Phytoremediation* **2016**, *18*, 348–353. [[CrossRef](#)]
21. Deng, T.-H.-B.; van der Ent, A.; Tang, Y.-T.; Sterckeman, T.; Echevarria, G.; Morel, J.-L.; Qiu, R.-L. Nickel Hyperaccumulation Mechanisms: A Review on the Current State of Knowledge. *Plant Soil* **2018**, *423*, 1–11. [[CrossRef](#)]
22. Mahar, A.; Wang, P.; Ali, A.; Awasthi, M.K.; Lahori, A.H.; Wang, Q.; Li, R.; Zhang, Z. Challenges and Opportunities in the Phytoremediation of Heavy Metals Contaminated Soils: A Review. *Ecotoxicol. Environ. Saf.* **2016**, *126*, 111–121. [[CrossRef](#)]
23. Sheoran, V.; Sheoran, A.S.; Poonia, P. Role of Hyperaccumulators in Phytoextraction of Metals from Contaminated Mining Sites: A Review. *Crit. Rev. Environ. Sci. Technol.* **2011**, *41*, 168–214. [[CrossRef](#)]
24. Sarma, H. Metal Hyperaccumulation in Plants: A Review Focusing on Phytoremediation Technology. *J. Environ. Sci. Technol.* **2011**, *4*, 118–138. [[CrossRef](#)]
25. Sinkala, T. Integrated Phytomining and Ethanol Production in the Zambian Copperbelt to Minimize Mine Decontamination Costs and Environmental and Social Impacts: A Review. *J. South. African Inst. Min. Metall.* **2018**, *118*, 815–824. [[CrossRef](#)]
26. Zhang, X.; Houzelot, V.; Bani, A.; Morel, J.L.; Echevarria, G.; Simonnot, M.O. Selection and Combustion of Ni-Hyperaccumulators for the Phytomining Process. *Int. J. Phytoremediat.* **2014**, *16*, 1058–1072. [[CrossRef](#)] [[PubMed](#)]
27. Barbaroux, R.; Mercier, G.; Blais, J.F.; Morel, J.L.; Simonnot, M.O. A New Method for Obtaining Nickel Metal from the Hyperaccumulator Plant *Alyssum Murale*. *Sep. Purif. Technol.* **2011**, *83*, 57–65. [[CrossRef](#)]
28. Broadhurst, C.L.; Chaney, R.L. Growth and Metal Accumulation of an *Alyssum Murale* Nickel Hyperaccumulator Ecotype Co-Cropped with *Alyssum Montanum* and Perennial Ryegrass in Serpentine Soil. *Front. Plant Sci.* **2016**, *7*, 1–9. [[CrossRef](#)] [[PubMed](#)]
29. Bani, A.; Echevarria, G.; Sulçe, S.; Morel, J.L. Improving the Agronomy of *Alyssum Murale* for Extensive Phytomining: A Five-Year Field Study. *Int. J. Phytoremediat.* **2015**, *17*, 117–127. [[CrossRef](#)] [[PubMed](#)]
30. Sellami, R.; Gharbi, F.; Rejeb, S.; Rejeb, M.N.; Henchi, B.; Echevarria, G.; Morel, J.L. Effects of Nickel Hyperaccumulation on Physiological Characteristics of *Alyssum Murale* Grown on Metal Contaminated Waste Amended Soil. *Int. J. Phytoremediat.* **2012**, *14*, 609–620. [[CrossRef](#)] [[PubMed](#)]
31. Galiová, M.V.; Száková, J.; Prokeš, L.; Čadková, Z.; Coufalík, P.; Kanický, V.; Otruba, V.; Tlustoš, P. Variability of Trace Element Distribution in *Noccaea* Spp., *Arabidopsis* Spp., and *Thlaspi Arvense* Leaves: The Role of Plant Species and Element Accumulation Ability. *Environ. Monit. Assess.* **2019**, *191*, 181. [[CrossRef](#)] [[PubMed](#)]
32. Bhatia, N.P.; Orlic, I.; Siegele, R.; Ashwath, N.; Baker, A.J.M.; Walsh, K.B. Elemental Mapping Using PIXE Shows the Main Pathway of Nickel Movement Is Principally Symplastic within the Fruit of the Hyperaccumulator *Stackhousia Tryonii*. *New Phytol.* **2003**, *160*, 479–488. [[CrossRef](#)]
33. Punshon, T.; Guerinet, M.L.; Lanzirotti, A. Using Synchrotron X-Ray Fluorescence Microprobes in the Study of Metal Homeostasis in Plants. *Ann. Bot.* **2009**, *103*, 665–672. [[CrossRef](#)]
34. Husted, S.; Persson, D.P.; Laursen, K.H.; Hansen, T.H.; Pedas, P.; Schiller, M.; Hegelund, J.N.; Schjoerring, J.K. Review: The Role of Atomic Spectrometry in Plant Science. *J. Anal. At. Spectrom.* **2011**, *26*, 52–79. [[CrossRef](#)]
35. Keeling, S.M.; Stewart, R.B.; Anderson, C.W.N.; Robinson, B.H. Nickel and Cobalt Phytoextraction by the Hyperaccumulator *Berkheya Coddii*: Implications for Polymetallic Phytomining and Phytoremediation. *Int. J. Phytoremediat.* **2003**, *5*, 235–244. [[CrossRef](#)] [[PubMed](#)]

36. Broadhurst, C.L.; Chaney, R.L.; Angle, J.S.; Erbe, E.F.; Mangel, T.K. Nickel Localization and Response to Increasing Ni Soil Levels in Leaves of the Ni Hyperaccumulator *Alyssum Murale*. *Plant Soil* **2004**, *265*, 225–242. [[CrossRef](#)]
37. Hunter, J.G.; Vergnano, O. Nickel and Cobalt Toxicities in Oat Plants. *Ann. Bot.* **1952**, *17*, 317–329.
38. Cabello-Conejo, M.I.; Centofanti, T.; Kidd, P.S.; Prieto-Fernández, Á.; Chaney, R.L. Evaluation of Plant Growth Regulators To Increase Nickel Phytoextraction By *Alyssum* Species. *Int. J. Phytoremediation* **2013**, *15*, 365–375. [[CrossRef](#)]
39. McNear, D.H.; Peltier, E.; Everhart, J.; Chaney, R.L.; Sutton, S.; Newville, M.; Rivers, M.; Sparks, D.L. Application of Quantitative Fluorescence and Absorption-Edge Computed Microtomography to Image Metal Compartmentalization in *Alyssum Murale*. *Environ. Sci. Technol.* **2005**, *39*, 2210–2218. [[CrossRef](#)]
40. Bolan, N.; Kunhikrishnan, A.; Thangarajan, R.; Kumpiene, J.; Park, J.; Makino, T.; Kirkham, M.B.; Scheckel, K. Remediation of Heavy Metal(Loid)s Contaminated Soils—To Mobilize or to Immobilize? *J. Hazard. Mater.* **2014**, *266*, 141–166. [[CrossRef](#)]
41. Diehl, M.; Evertz, M.; Winter, M.; Nowak, S. Deciphering the Lithium Ion Movement in Lithium Ion Batteries: Determination of the Isotopic Abundances of ⁶Li and ⁷Li. *RSC Adv.* **2019**, *9*, 12055–12062. [[CrossRef](#)]
42. Harte, P.; Evertz, M.; Schwieters, T.; Diehl, M.; Winter, M.; Nowak, S. Adaptation and Improvement of an Elemental Mapping Method for Lithium Ion Battery Electrodes and Separators by Means of Laser Ablation-Inductively Coupled Plasma-Mass Spectrometry. *Anal. Bioanal. Chem.* **2019**, *411*, 581–589. [[CrossRef](#)]



© 2020 by the authors. Licensee MDPI, Basel, Switzerland. This article is an open access article distributed under the terms and conditions of the Creative Commons Attribution (CC BY) license (<http://creativecommons.org/licenses/by/4.0/>).